Highly Efficient Plasmon-Enhanced Dye-Sensitized Solar Cells through Metal@Oxide Core–Shell Nanostructure

Jifa Qi,[†,‡,§] Xiangnan Dang,[†,‡,§] Paula T. Hammond,[‡,⊥,*] and Angela M. Belcher[†,‡,∥,*]

[†]Department of Materials Science and Engineering, Massachusetts Institute of Technology, Cambridge, Massachusetts 02139, United States,
[‡]The David H. Koch Institute for Integrative Cancer Research, Massachusetts Institute of Technology, Cambridge, Massachusetts 02139, United States,
[⊥]Department of Chemical Engineering, Massachusetts Institute of Technology, Cambridge, Massachusetts 02139, United States, and
[∥]Department of Biological Engineering, Massachusetts Institute of Technology, Cambridge, Massachusetts 02139, United States.
[§]These authors contributed equally to this work.

ABSTRACT We have investigated the effects of localized surface plasmons (LSPs) on the performance of dye-sensitized solar cells (DSSCs). The LSPs from Ag nanoparticles (NPs) increase the absorption of the dye molecules, allowing us to decrease the thickness of photoanodes, which improves electron collection and device performance. The plasmon-enhanced DSSCs became feasible through incorporating core–shell Ag@TiO_2 NPs into conventional TiO_2 photoanodes. The thin shell keeps the photoelectrons from recombining on the surface of metal NPs with dye and electrolyte and improves the stability of metal NPs. With 0.6 wt % Ag@TiO_2 NPs, the power conversion efficiency of DSSCs with thin photoanodes (1.5 μm) increases from 3.1% to 4.4%. Moreover, a small amount of Ag@TiO_2 NPs (0.1 wt %) improves efficiency from 7.8% to 9.0% while decreasing photoanode thickness by 25% for improved electron collection. In addition, plasmon-enhanced DSSCs require 62% less material to maintain the same efficiency as conventional DSSCs.

KEYWORDS: dye-sensitized solar cells · photovoltaics · silver nanoparticles · surface plasmon · absorption enhancement · titanium dioxide · core–shell nanostructures

Dye-sensitized solar cells (DSSCs), consisting of a mesoporous TiO_2 film covered by a monolayer of charge-transfer dye molecules, have attracted great attention for high power conversion efficiency (PCE) up to 11% and the low cost of materials and fabrication processes.[1–5] To improve the PCE of DSSCs, conventional approaches include enhancing absorption of incident light[2,5] and improving collection of photogenerated carriers.[6,7] By changing the thickness or morphology (*e.g.*, vertically aligned ZnO[6] or TiO_2[7] nanowire arrays) of the photoanode, the light absorption and carrier collection, however, are often affected in opposite ways. Effort has also been devoted to developing new dyes[8–10] and using semiconductor quantum dots.[11,12] Nevertheless, employing new dyes or quantum dots could change the adsorption of the sensitizers on TiO_2, as well as their energy band positions relative to the conduction band of TiO_2 and the redox potential of the electrolyte, affecting charge separation. Therefore, improving light harvest or carrier collection without affecting other factors has been considered a more effective approach to improve device performance.[13] Localized surface plasmons (LSPs) have potential for improving the performance of DSSCs for the unique capability to improve the light absorption of dye with minimal impact on other material properties.

Generally, there are three types of plasmonic light-trapping geometries,[14] including far-field scattering, near-field LSPs, and surface plasmon polaritons at the metal/semiconductor interface. Surface plasmon arising from metal nanoparticles (NPs) has been applied to increase the optical absorption and/or photocurrent in a wide range of solar cell configurations, *e.g.*, silicon solar cells,[15–18] organic solar cells,[19–21] organic bulk heterojunction solar cells,[22] CdSe/Si heterostructures,[23] and DSSCs.[24–32] However, most of the previous work on plasmon-enhanced DSSCs reported only improved dye absorption or photocurrent, while the improved device performance was not observed.[24–28] In addition, the earlier plasmonic geometries contained metal NPs in direct contact with the dye and the electrolyte,[24–26,29,30] resulting in recombination and back reaction of photogenerated carriers and corrosion of metal NPs by electrolytes. Recently core–shell Au@SiO_2 NPs have been applied to achieve enhanced PCE by preventing the recombination and back reaction.[32] However, by using an insulating shell, part of the photogenerated carriers from the most absorption-enhanced dye molecules located on the surfaces of SiO_2 would be lost due to the difficulty in the injection to SiO_2.

* Address correspondence to hammond@mit.edu, belcher@mit.edu.

Received for review May 17, 2011 and accepted July 29, 2011.

Published online August 04, 2011
10.1021/nn201808g

Here we report an approach toward plasmon-enhanced DSSCs by incorporating Ag@TiO_2 nanostructures into the TiO_2 photoanode. Our approach is demonstrated with the following advantages. First, a shell covering metal NPs is utilized to prevent recombination and back reaction, protecting metal NPs during device fabrication, as well as preventing metal NPs from corrosion by electrolytes. Second, we choose TiO_2 rather than insulating components as the shell material because the carriers can be easily transferred to surrounding TiO_2 nanoparticles that are in contact with the shell. Third, in order to maximize the effect of LSPs, we use a small Ag core and a very thin shell of TiO_2 (2 nm). By utilizing Ag@TiO_2 core–shell nanostructures, we demonstrate that the optical absorption of dye molecules in solution and thin film is enhanced by the strong localized electric field generated by LSPs. By incorporating Ag@TiO_2 NPs, the PCE of DSSCs with very thin photoanodes (1.5 μm) is increased from 3.1% to 4.4%. Moreover, a small amount of Ag@TiO_2 NPs (0.1 wt %) improved efficiency from 7.8% to 9.0% while decreasing the photoanode thickness by 25% for improved electron collection. In addition, 62% less material is required for plasmon-enhanced DSSCs to maintain the same efficiency as conventional DSSCs (6.5%).

RESULTS AND DISCUSSION

The structure and mechanism for the conventional and plasmon-enhanced DSSCs are shown in Figure 1a–d. In the conventional DSSCs, the dyes absorb incident light and generate electrons in excited states, which inject into the TiO_2 NPs. The oxidized dye molecules are regenerated by electrons transferred from iodide. The regenerative cycle is completed by reducing triiodide to iodide at the Pt cathode. The electrons in TiO_2 diffuse to the current collector (fluorine-doped tin oxide, FTO). In the plasmon-enhanced DSSCs, the LSPs arising from Ag@TiO_2 NPs increase dye absorption, allowing us to decrease the thickness of photoanode. By decreasing the thickness of photoanode, less material is required, and the recombination as well as back reaction of photocarriers is reduced, which improves the electron collection efficiency and thus the device performance. The core–shell nanostructure is crucial for plasmon-enhanced DSSCs, as shown in Figure 1e,f, since the oxide shell reduces the recombination and back reaction of electrons on the surface of metal NPs by providing an energy barrier between metal and dye/electrolyte. The oxide layer also protects metal NPs from etching by the electrolyte.

Geometric Design and Synthesis of Core–Shell Nanostructure of Ag@TiO_2. The induced electric field of the surface plasmon of a metal NP strongly depends on the radial distance, r, from the NP:[33,34]

$$E_{out}(r) = E_0\hat{z} - \left[\frac{\varepsilon_{in} - \varepsilon_{out}}{\varepsilon_{in} + 2\varepsilon_{out}}\right] a^3 E_0 \left[\frac{\hat{z}}{r^3} - \frac{3z}{r^5} r\right] \quad (1)$$

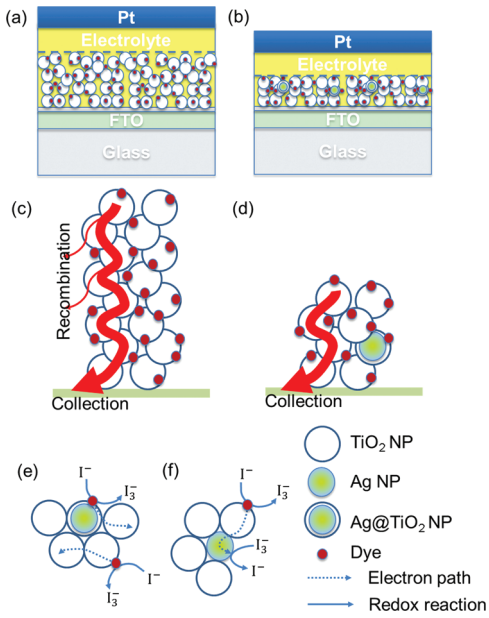

Figure 1. Structures and mechanisms of conventional DSSCs and plasmon-enhanced DSSCs. Device structures of conventional DSSCs (a) and plasmon-enhanced DSSCs (b); plamson-enhanced DSSCs require thinner film and less material to achieve the same PCE. Illustration of photogenerated electron collection in conventional DSSCs (c) and plasmon-enhanced DSSCs (d); plasmon-enhanced DSSCs avoid electron recombination due to thinner photoanode layer. Mechanisms of plasmon-enhanced DSSCs using Ag@TiO_2 NPs (e) and Ag NPs (f), while using Ag@TiO_2 NPs, optical absorption of dye molecules is enhanced by LSPs, electrons diffuse among TiO_2 NPs, and iodide ions regenerate dyes by providing electrons, and while using Ag NPs, there is direct contact between Ag and the electrolyte and the surface of Ag NPs serves as a recombination site for the photogenerated electrons and triiodide ions.

where E_0 and E_{out} are the electric field of incident light and the electric field outside the metal NP; ε_{in} and ε_{out} are the dielectric constant of the metal NP and that of the external environment; and a is the radius of the spherical metal NP. The surface plasmon-induced electric field decreases quickly with increasing distance from the NP. Therefore, a thinner shell corresponds to a stronger electric field induced by LSPs on or close to the surface of the core–shell NP, thus more absorption enhancement of the dye molecules surrounding the core–shell NP (experimental evidence can be found in Supporting Information Figures S1 and S2). In addition, LSPs play a dominant role only when the NP size is much smaller than the wavelength of incident light, since larger metal NPs scatter light more. Therefore, we utilize the core–shell nanostructure with a small metal core and a thin oxide shell, *i.e.*, Ag@TiO_2 nanostructure, to maximize the effects of LSPs on optical absorption of dye molecules and the performance of DSSCs. We synthesized Ag@TiO_2 NPs using a two-step chemical reaction, forming Ag NPs at 120 °C and forming TiO_2 shells at room temperature (see Materials and Methods). Figure 2a shows the transmission electron microscope (TEM) image of Ag@TiO_2 NPs, and

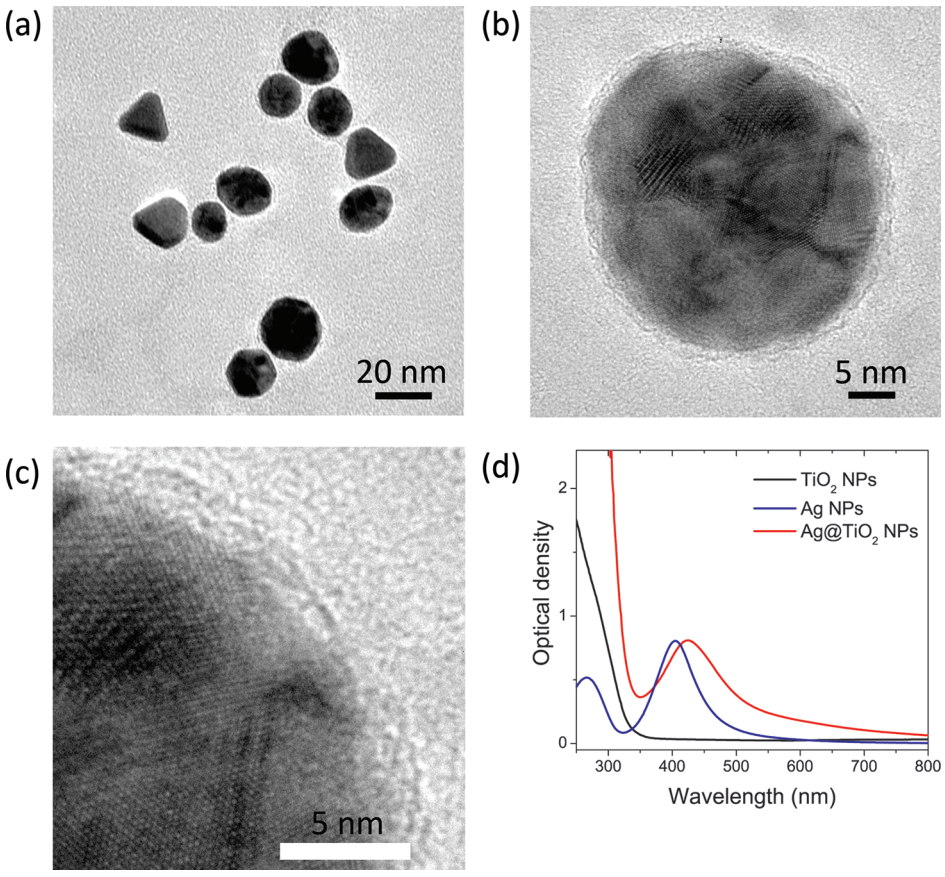

Figure 2. Synthesis and characterization of Ag@TiO_2 NPs. (a–c) TEM and HRTEM images of Ag@TiO_2 NPs. (d) Optical absorption spectra of solutions of Ag NPs stabilized by PVP (average molecular weight 10 000), TiO_2 NPs, and Ag@TiO_2 NPs.

Figure 2b,c show the high-resolution TEM (HRTEM) images of an individual Ag@TiO_2 NP with the lattice fringes of Ag crystalline structure and an amorphous TiO_2 shell about 2 nm thick. The formation of Ag@TiO_2 nanostructure was also confirmed by optical absorption spectroscopy (Figure 2d). The absorption peak from the surface plasmon resonance shifts from 403 nm to a longer wavelength of 421 nm, due to the higher dielectric constant surrounding the Ag NPs of amorphous TiO_2 than that of polyvinylpyrrolidone (PVP).

To investigate the stability of Ag@TiO_2 NPs during device fabrication, we examined the structure of the core–shell NPs before and after the annealing process through X-ray diffraction (XRD). Figure 3 shows XRD patterns of Ag@TiO_2 NPs as-synthesized and annealed at 500 °C. For the core–shell NPs as-synthesized at room temperature, the diffraction patterns from (111), (200), (220), and (311) planes of cubic structured Ag NPs were clearly seen, while a broad peak at 22.4° was ascribed to the X-ray scattering from the amorphous-structured TiO_2 shells. After annealing, the broad amorphous peak disappeared, while the diffraction patterns from (101), (200), (105), and (211) planes of anatase-structured TiO_2 shells were observed. The crystallinity of the Ag NPs was also improved by annealing, observed by both XRD and

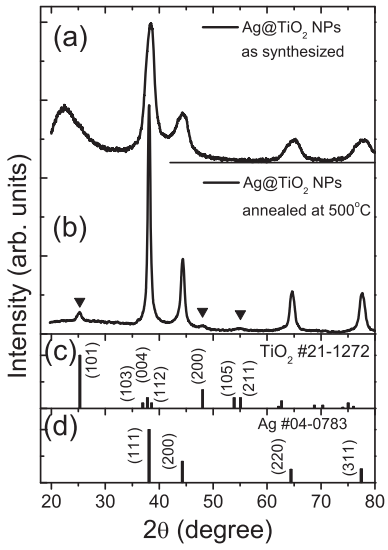

Figure 3. XRD patterns of Ag@TiO_2 NPs as-synthesized at room temperature (a) and after annealing at 500 °C for 30 min (b). The inverted triangle symbols indicate the XRD patterns from anatase-structured TiO_2. (c, d) The XRD patterns based on the JCPDS card for anatase TiO_2 (#21-1272) and Ag (#04-0783), respectively.

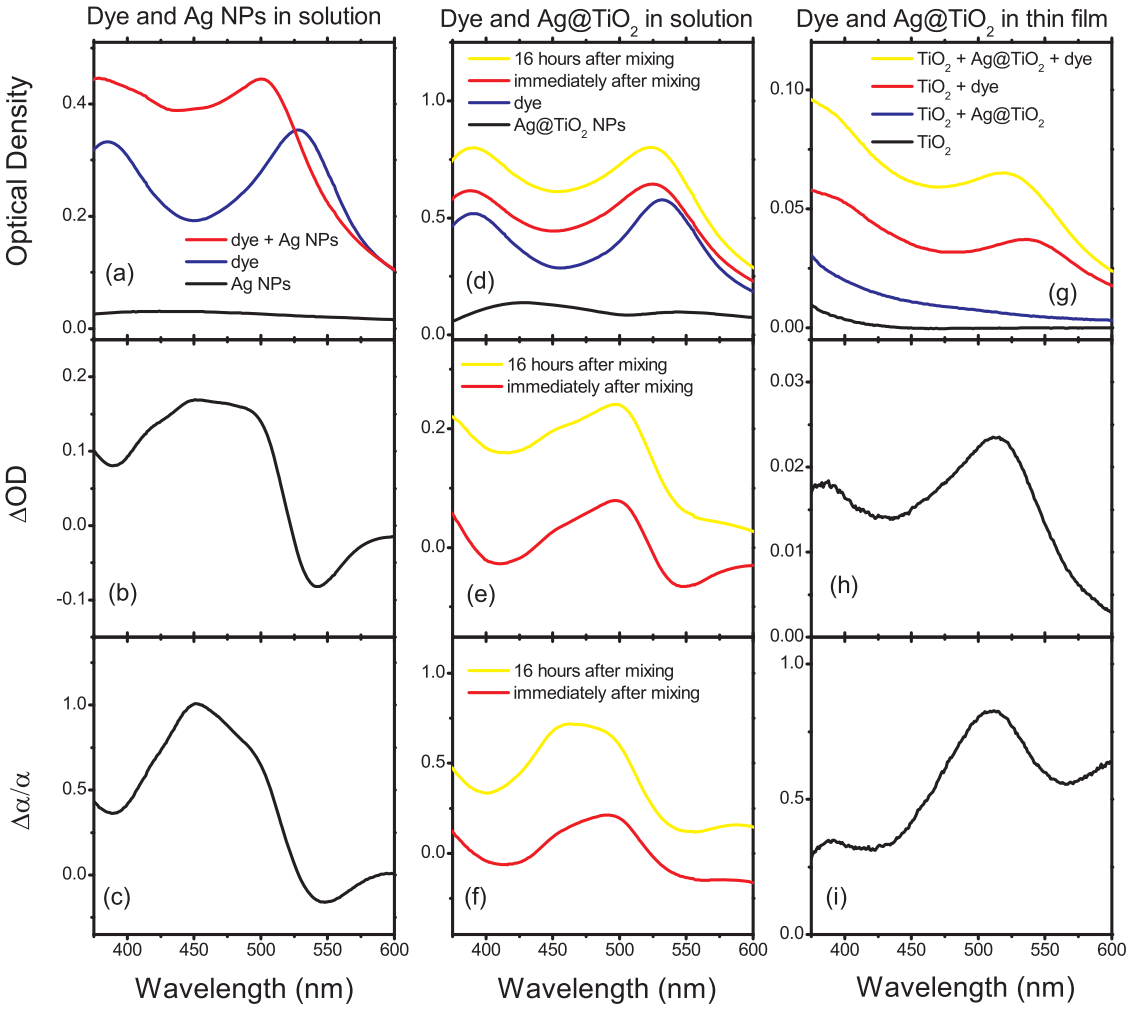

Figure 4. LSP-induced enhancement of optical absorption of dye molecules in solution and thin film. (a) Optical absorption spectra of Ag NPs, ruthenium dye molecules, and their mixture in ethanol solution. (b) Net changes of dye absorption (ΔOD) due to the presence of Ag NPs in solution. (c) Relative changes of effective extinction coefficient of dye ($\Delta\alpha/\alpha$) due to the presence of Ag NPs in solution. (d) Optical absorption spectra of Ag@TiO_2 NPs, ruthenium dye molecules, and their mixtures (immediately after mixing and 16 h after mixing) in ethanol solution. (e) Net changes of dye absorption (ΔOD) due to the presence of Ag@TiO_2 NPs in solution. (f) Relative changes of effective extinction coefficient of dye ($\Delta\alpha/\alpha$) due to the presence of Ag@TiO_2 NPs in solution. (g) Optical absorption spectra of Ag@TiO_2 NPs, ruthenium dye molecules, and their mixtures in the matrix of TiO_2 thin film. (h) Net changes of dye absorption (ΔOD) due to the presence of Ag@TiO_2 NPs in thin film. (i) Relative changes of effective extinction coefficient of dye ($\Delta\alpha/\alpha$) due to the presence of Ag@TiO_2 NPs in thin film. For the calculation of ΔOD and $\Delta\alpha/\alpha$: $\Delta\alpha/\alpha = \Delta OD(\lambda)/OD_{dye}(\lambda) = (OD_{dye,Ag}(\lambda) - OD_{dye}(\lambda) - OD_{Ag}(\lambda))/OD_{dye}(\lambda)$, where $OD_{dye}(\lambda)$, $OD_{Ag}(\lambda)$, and $OD_{dye,Ag}(\lambda)$ are the optical densities at wavelength λ of pure dye solution, Ag NP solution, and their mixture solution with the same concentrations of dye and Ag NPs, respectively. For the solid-state thin films, the net absorption of dye molecule is $OD_{dye}(\lambda) = OD_{dye,TiO2}(\lambda) - OD_{TiO2}(\lambda)$.

HRTEM. It is considered that the shell layer protects the Ag cores from reacting with the environment or aggregating to form larger particles during the annealing process. In addition, the shell layer is also considered to protect the Ag cores from corrosion by the electrolyte during solar cell operation.

Effect of LSPs on the Optical Absorption of Dye Molecule. The effect of LSPs from metal NPs on the absorption of ruthenium dye is investigated in both solution and thin film. At first, we studied the LSP effect on dye absorption in the solution of dye and Ag or Ag@TiO_2 NPs. The LSP effect in solution simulates the effect in plasmon-enhanced DSSCs, and the concentrations of NPs and dyes can be precisely controlled. As shown in Figure 4a–c, the absorption of dye increases with the presence of Ag NPs in solution, and the absorption peak position shifts from 530 nm to a shorter wavelength of 510 nm (Figure 4a). The maximum relative enhancement of dye absorption occurs at 450 nm (Figure 4c), close to the LSP resonance peak of Ag NPs around 403 nm instead of the dye absorption peak at 535 nm, suggesting that the increase of dye absorption mainly arises from LSPs of Ag NPs. Figure 4d–f show that the dye absorption in solution can also be enhanced by incorporating Ag@TiO_2 NPs. Moreover, this enhancement of dye absorption increases with time after mixing dye and core–shell NPs (Figure 4d), which could be the effect of the dye molecules adsorbing on the surface of

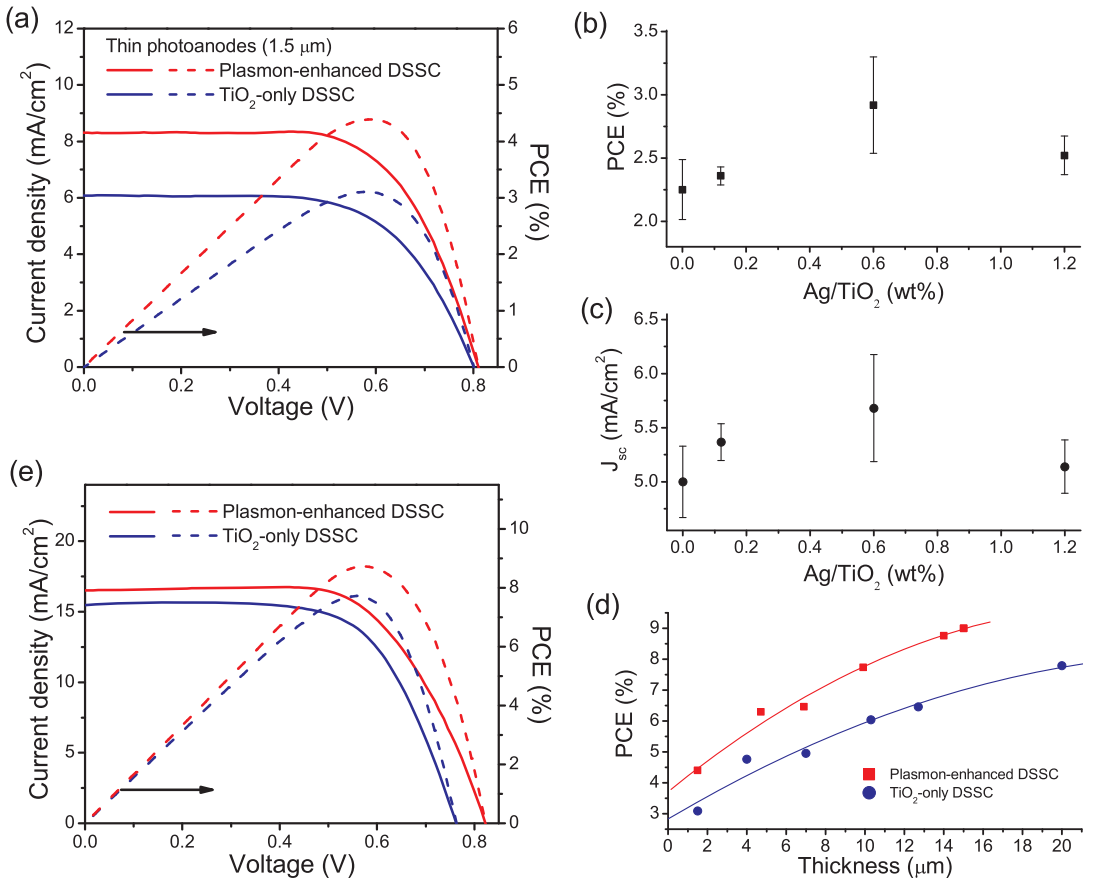

Figure 5. Effect of LSPs on the performance of DSSCs. (a) Current density (solid lines) and PCE (dashed lines) of the plasmon-enhanced DSSC (Ag/TiO_2 = 0.6 wt %, η = 4.4%, FF = 66%) and TiO_2-only DSSC (η = 3.1%, FF = 64%) with the same photoanode thickness of 1.5 μm; (b, c) dependence of PCE and J_{SC} on the concentration of Ag@TiO_2 NPs in a photoanode with the same thickness of 1.5 μm; (d) PCE of plasmon-enhanced DSSC and TiO_2-only DSSC with photoanodes of different thickness, where the lines are drawn to show the tendency; (e) current density (solid lines) and PCE (dashed lines) of the most efficient plasmon-enhanced DSSC (Ag/TiO_2 = 0.1 wt %, η = 9.0%, FF = 67%, 15 μm) and TiO_2-only DSSC (η = 7.8%, FF = 66%, 20 μm) in this work.

the TiO_2 shell. While increasing the time after mixing, the number of dye molecules adsorbed on the Ag@TiO_2 NPs increases, reducing the average distance between dye molecules and Ag cores, thus further enhancing the dye absorption. This time-dependent (dye-to-NP distance-dependent) behavior of absorption enhancement agrees with our intention of utilizing a thin shell to maximize the LSP effect. In addition, the adsorption of dye on Ag@TiO_2 in solution is similar to that in the thin films, where the dye molecules are adsorbed on or near the surface of Ag@TiO_2 NPs. In order to study the LSP effect on the absorption of dye molecules in mesoporous TiO_2 thin films, 1 μm thick films were prepared by spin-coating TiO_2 NPs and TiO_2 NPs blended with Ag@TiO_2 NPs (Ag:TiO_2 = 0.2 wt %) and annealed at 500 °C (see Materials and Methods). Compared to the dyed TiO_2 film, there is an increase of absorption for the film incorporated with Ag@TiO_2 NPs (Figure 4g), and the enhancement is similar to that in the solution (Figure 4i). It also agrees with the previously reported observations on plasmon-enhanced dye absorption.[24,25,27,28,32] The increase of absorption of dye molecules could be attributed to the interaction of dye molecular dipole and enhanced electric field surrounding the NPs, together with the increase of light scattering also induced by LSPs, which increased the optical path.

Effect of LSPs on the Performance of DSSCs. To investigate the effect of LSPs on device performance, we compared the performance of plasmon-enhanced DSSCs and standard DSSCs with only TiO_2 NPs as photoanodes. The TiO_2-only DSSCs were fabricated using the conventional method,[13] while the Ag@TiO_2 NPs (0.02 to 1.2 wt %) were incorporated into TiO_2 paste to fabricate the plasmon-enhanced DSSCs (see Materials and Methods). Figure 5a shows the photocurrent density−voltage characteristics (J−V curves) of the most efficient plasmon-enhanced DSSC and TiO_2-only DSSC with the same photoanode thickness of 1.5 μm. The TiO_2-only DSSC showed a PCE (η) of 3.1%, whereas the plasmon-enhanced DSSC with Ag@TiO_2 NPs exhibited a PCE of 4.4% (increased by 42%). Compared with the TiO_2-only DSSC, the fill factor (FF) and open-circuit voltage (V_{OC}) of the plasmon-enhanced DSSC were close, while the short-circuit current density (J_{sc}) significantly increased by 37%, from 6.07 mA/cm^2 to

8.31 mA/cm^2. Since $\eta = J_{SC}V_{OC}FF/P_0$, where P_0 is the intensity of incident light, the improvement of PCE in the plasmon-enhanced DSSC is mainly due to the increased photocurrent corresponding to enhanced dye absorption by LSPs. We further investigated the effect of the concentration of Ag@TiO_2 on the device performance. Figure 5b,c show the averaged PCE and J_{SC} changing with concentration of Ag@TiO_2 NPs. When the concentration of Ag/TiO_2 increased from 0 to 0.6 wt %, both J_{SC} and PCE monotonically increased. The decrease of PCE was observed with further increasing Ag@TiO_2 concentration, which was probably due to the increased trapping of photogenerated electrons by Ag and increased light absorption of Ag NPs, which transformed part of the incident solar power into heat. Therefore, through enhancing the light absorption and photocurrent, the device performance of DSSCs has been improved by LSPs from Ag@TiO_2 NPs. To our knowledge, a PCE of 4.4% is the best performance for DSSCs with photoanodes of similar thicknesses.

For practical DSSCs, thicker photoanodes are required to absorb more light. By using LSPs, the thickness of the photoanodes can be reduced while maintaining the optical absorption of the DSSC. As shown in Figure 5d, the PCE of DSSCs increases with the thickness for both conventional and plasmon-enhanced DSSCs, but it increases faster with the presence of Ag@TiO_2 NPs in the photoanode. For devices with the same thickness, the PCE of the plasmon-enhanced DSSC is higher than that of the TiO_2-only DSSC. In addition, to achieve the same PCE, the photoanode thickness of the plasmon-enhanced DSSC is much thinner than that of the TiO_2-only DSSC. For instance, it is observed that the plasmon-enhanced DSSC with a 5 μm thick photoanode and the TiO_2-only DSSC with a 13 μm thick photoanode possess the same PCE of 6.5%, reducing by 62% the material used for device fabrication without affecting the device performance.

Electron collection is also an important factor to be considered in addition to light harvesting, since light absorption in practical devices is near unity with thicker photoanodes. Although the optical absorption is increased by thicker photoanodes, the carrier collection efficiency is decreased due to longer distance for electron diffusion. In contrast, a thinner photoanode with the same optical absorption, enabled by LSPs, is expected to be advantageous to the electron collection as well as the device performance. As shown in Figure 5e, the plasmon-enhanced DSSC achieved the highest PCE of 9.0% with a 15 μm thick photoanode, compared to the TiO_2-only DSSC, reaching the highest PCE of 7.8% with a 20 μm thick photoanode. Therefore, by introducing Ag@TiO_2 NPs into the TiO_2 photoanode, the PCE of the DSSC was improved by 15% while the photoanode thickness was decreased by 25%. Considering the near-unity optical absorption for the photoanodes of both plasmon-enhanced and TiO_2-only DSSCs, the improved PCE mostly arises from increased electron collection efficiency by decreased distance for electron diffusion. In addition, the uniform plasmonic geometry employed enhances the absorption throughout the photoanode, whereas the metal NPs from previous works were located either on the current collector[23−28] or on the counter electrode,[29] where the LSP affected only the thin layer close to the metal NPs.

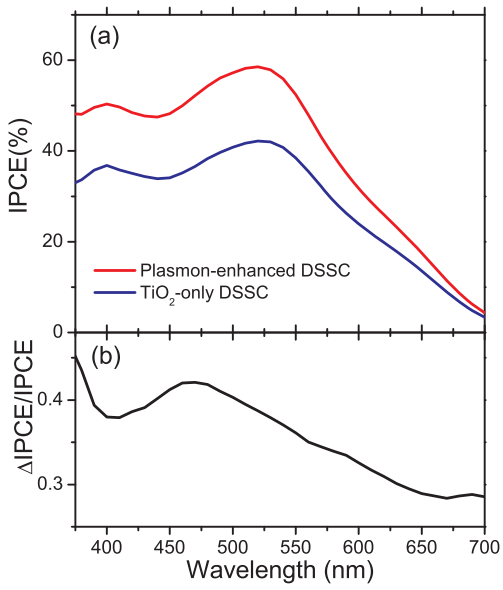

Figure 6. Spectral responses of TiO_2-only and plasmon-enhanced DSSCs. (a) IPCE spectra of the DSSCs with and without the presence of Ag@TiO_2; (b) the relative change of the IPCE caused by the incorporation of Ag@TiO_2 NPs. $\Delta IPCE/IPCE(\lambda) = (IPCE_{plasmon\text{-}enhanced}(\lambda) - IPCE_{TiO2\text{-}only}(\lambda))/IPCE_{TiO2\text{-}only}(\lambda)$, where $IPCE_{plasmon\text{-}enhanced}(\lambda)$ and $IPCE_{TiO2\text{-}only}(\lambda)$ are the ICPE at wavelength λ for plasmon-enhanced DSSC and TiO_2-only DSSC, respectively.

To investigate the effect of LSPs on the spectral response of solar cells, the incident photon-to-current efficiency (IPCE) measurement was performed (Figure 6). The IPCE is the product of the light-harvesting efficiency, electron injection efficiency, and electron collection efficiency. Increasing light absorption will directly improve light harvesting and the IPCE, if electron injection and collection are not affected. As shown in Figure 6a, the shape of the IPCE spectrum from the TiO_2-only device closely matches the shape of optical absorption of the dye molecules in the thin film, while the IPCE spectrum from the plasmon-enhanced device increases over the whole wavelength range. Moreover, the enhancement is most significant in the range 400−500 nm with a peak around 460 nm (Figure 6b). The similarity between IPCE enhancement of the DSSC and the absorption enhancement of the thin film indicates that the LSPs from core−shell NPs improved the device performance through increased dye absorption.

CONCLUSION

We developed a general approach to utilizing LSPs to improve the performance of DSSCs. We demonstrated

that the enhanced localized electromagnetic field increased the optical absorption of dye molecules in solution and in thin films. By incorporating small Ag NPs coated with a thin TiO_2 shell into the TiO_2 photoanodes as thin as 1.5 μm, we achieved a PCE of 4.4%, and the best plasmon-enhanced DSSC in our work had a PCE of 9.0% with reduced photoanode thickness for better electron collection. Our method has the advantages of preventing charge recombination at the surface of metal NPs, improving thermal and chemical stability of metal cores, and uniformly enhancing optical absorption throughout the photoanode. In addition, the fabrication method for plasmon-enhanced DSSCs is compatible with large-scale processes, such as printing and jet-spraying.

We believe that the implications of our work will guide the research in utilizing LSPs to improve practical DSSC performance, by reducing the photoanode thickness while retaining the near-unity absorption, thus improving electron collection and PCE. Moreover, molecular dyes possessing improved charge separation and better stability against water and oxygen in the environment could be employed in DSSCs without the requirement of high light extinction due to enhanced dye absorption by LSPs. Our approach also enables the utilization of LSPs in many other thin-film photovoltaic technologies that require efficient light harvesting and decreased recombination and back reaction, such as quantum dot-sensitized solar cells, organic solar cells, and quantum dot/organic hybrid solar cells, and other types of photoelectron conversion devices, such as photodetectors.

MATERIALS AND METHODS

Materials. Titanium isopropoxide (TPO, 97%) and polyvinylpyrrolidone with an average molecular weight of 10 000 (PVP-10) were purchased from Sigma-Aldrich; ethanol (99.5%), acetone (99.5%), nitric acid (70%), and ethylene glycol (99.9%) were purchased from Mallinckrodt Chemicals; ammonia (28−30 wt % NH_3 in water) was purchase from VWR International Inc. Poly(acrylic acid) (PAA, average molecular weight 90 000, 25% aqueous solution) was obtained from Polysciences, Inc. *cis*-Bis(isothiocyanato)bis(2,2′-bipyridyl-4,4′-dicarboxylato)ruthenium-(II) (also named N3 or Ruthenizer 535, purchased from Solaronix) was used as a 0.5 mM solution in acetonitrile and *tert*-butanol (volume ratio = 1:1). All chemicals were used as received. All water was deionized (18.2 MΩ, milli-Q pore).

Synthesis of NPs. The 20 nm sized TiO_2 nanocrystals were synthesized using the procedure in the literature.[5] Small Ag NPs with a diameter of 20−30 nm were synthesized by a modified polyol process: typically, 0.1 mmol of silver nitrate was added into 25 mL of ethylene glycol solution containing 0.5 g of PVP-10, and the mixture was kept stirring at room temperature until the silver nitrate was completely dissolved. Then the solution was slowly heated up to 120 °C and kept at that temperature for 1 h with constant stirring. After the reaction, the NPs were separated from ethylene glycol by addition of acetone (200 mL of acetone per 25 mL of reaction mixture) and subsequent centrifugation at 3000 rpm. The supernatant was removed, and the NPs were washed with ethanol, centrifuged at 3000 rpm, and redispersed in 18 mL of ethanol and 2 mL of 4% ammonia in ethanol (achieved by diluting the 28% ammonia seven times in ethanol). This solution was stirred and sonicated more than 30 min and divided equally into two parts, which were directly used for coating the TiO_2 shell by adding TPO solution in ethanol while stirring the solution vigorously. Typically, 6 μL of TPO in 1 mL of ethanol was added into the solution, yielding a shell of TiO_2 around 2 nm thick. The reaction mixture was then stirred for 12 h at room temperature in the dark. The Ag NPs in ethylene glycol (as synthesized) or in ethanol (purified) both can be used for synthesis of Ag@TiO_2 NPs with thicker TiO_2 shells. A solution of PAA was prepared by adding 2 g of PAA (25% aqueous solution) into a mixed solvent of 1 mL of water and 8 mL of ethanol and stirring at room temperature for over 1 h. Then 0.2 mL of PAA solution was added into 12.5 mL of the as-synthesized Ag NPs in ethylene glycol (containing 0.05 mmol of Ag) or into 10 mL of Ag NPs in ethanol (containing less than 0.05 mmol of Ag due to the loss during purification), and the solution was kept stirring for over 4 h and sonicated for 30 min at room temperature. Then 1 mL of ethanol solution containing 20 μL of TPO was added into the Ag NP solution, and the reaction was kept stirring in the dark. The TEM images of Ag@TiO_2 NPs after reacting with TPO for 2 h are shown in Figure S1 (Supporting Information).

Characterization of NPs. TEM observations of synthesized nanostructures (TiO_2, Ag, and Ag@TiO_2) were performed using JEOL 200CX, JEOL 2011, and JEOL 2010F TEMs with an accelerating voltage of 200 kV. The optical absorption spectroscopy measurements were performed using a Beckman Coulter DU800 UV−vis spectrophotometer. One micrometer thick films of TiO_2 NPs or TiO_2 NPs incorporated with Ag@TiO_2 NPs on 2.5 × 2.5 cm^2 fused silica wafers were used for thin-film optical absorption measurements, which were prepared by spin coating (Specialty Coating Systems, 6800 spin coater) and followed by annealing treatment at 500 °C for 15 min. Then the film thickness was measured using a Dektak 150 surface profiler. These films were immersed into 0.1 mM ruthenium dye solution (volume ratio of acetonitrile to *tert*-butanol is 1:1) and kept at room temperature for 12 h. Then the dyed films were immersed in acetonitrile for 5 min to remove nonadsorbed dye.

Fabrication of DSSCs. The fabrication of the 1.5 μm thick photoanodes of both TiO_2-only DSSCs and plasmon-enhanced DSSCs was performed by spin coating, the same method used for preparing thin films for optical absorption measurement. For TiO_2-only DSSCs with a photoanode thickness larger than 1.5 μm, the fabrication was carried out using the procedure described previously.[13] The photoanodes incorporated with Ag@TiO_2 NPs were fabricated with a modified procedure. The different amounts of Ag@TiO_2 NPs in ethanol solution (Ag to TiO_2 ratio from 0.02 to 1.2 wt %) were mixed with TiO_2 paste (mixture of TiO_2 NPs, ethyl celluloses, and terpinol), followed by stirring and sonicating. Then ethanol was removed by a rotary-evaporator. After the paste incorporated with Ag@TiO_2 NPs was achieved, the fabrication procedure of the photoanodes of plasmon-enhanced DSSCs was the same as that of the TiO_2-only DSSCs. The photoanodes of TiO_2-only and those incorporated with Ag@TiO_2 were immersed into N3 dye solution and kept at room temperature for 24 h. Then dyed films were immersed in acetonitrile for 5 min to remove nonadsorbed dye.

Characterization of DSSCs. Photovoltaic measurements were performed under illumination generated by an AM 1.5 solar simulator (Photo Emission Tech.). The power of the simulated light was calibrated to 100 mW/cm^2 by using a reference Si photodiode with a powermeter (1835-C, Newport) and a reference Si solar cell in order to reduce the mismatch between the simulated light and AM 1.5. The *J*−*V* curves were obtained by applying an external bias to the cell and measuring the

generated photocurrent with a Keithley model 2400 digital source meter. The voltage step and delay time of the photocurrent were 10 mV and 40 ms, respectively. A black tape mask was attached to the device in order to prevent irradiations from scattered light. The IPCE spectra were obtained using a computer-controlled system (Mode QEX7, PV Measurements Inc.) consisting of a 150 W xenon lamp light source and a monochromator equipped with two 1200 g/mm diffraction gratings. The incident photon flux was determined using a calibrated silicon photodiode. Measurements were performed in a short-circuit condition, while the cell was under background illumination from a bias light of 50 mW/cm^2.

Acknowledgment. This work was supported by Eni, S.p.A (Italy) through the MIT Energy Initiative Program.

Supporting Information Available: TEM characterization of Ag@TiO_2 with a thick TiO_2 shell and device performance of plasmon-enhanced DSSC using Ag@TiO_2 with a thick TiO_2 shell. This material is available free of charge *via* the Internet at http://pubs.acs.org.

REFERENCES AND NOTES

1. O'Regan, B.; Grätzel, M. A Low-Cost, High-Efficiency Solar Cell Based on Dye-Sensitized Colloidal TiO_2 Films. *Nature* **1991**, *353*, 737–740.
2. Nazeeruddin, M. K.; Kay, A.; Rodicio, I.; Humphry-Baker, R.; Mueller, E.; Liska, P.; Vlachopoulos, N.; Grätzel, M. Conversion of Light to Electricity by *cis*-X_2bis(2,2′-bipyridyl-4,4′-dicarboxylate)ruthenium(II) Charge-Transfer Sensitizers (X = Cl^-, Br^-, I^-, CN^-, and SCN^-) on Nanocrystalline Titanium Dioxide Electrodes. *J. Am. Chem. Soc.* **1993**, *115*, 6382–6390.
3. Grätzel, M. Photoelectrochemical Cells. *Nature* **2001**, *414*, 338–344.
4. Grätzel, M. Dye-Sensitized Solar Cells. *J. Photochem. Photobiol. A: Photochem. Rev.* **2003**, *4*, 145–153.
5. Chen, C.-Y.; Wang, M.; Li, J.-Y.; Pootrakulchote, N.; Alibabaei, L.; Ngoc-le, C.-h.; Decoppet, J.-D.; Tsai, J.-H.; Grätzel, C.; Wu, C.-G.; *et al.* Highly Efficient Light-Harvesting Ruthenium Sensitizer for Thin-Film Dye-Sensitized Solar Cells. *ACS Nano* **2009**, *3*, 3103–3109.
6. Law, M.; Greene, L. E.; Johnson, J. C.; Saykally, R.; Yang, P. Nanowire Dye-Sensitized Solar Cells. *Nat. Mater.* **2005**, *4*, 455–459.
7. Varghese, O. K.; Paulose, M.; Grimes, C. A. Long Vertically Aligned Titania Nanotubes on Transparent Conducting Oxide for Highly Efficient Solar Cells. *Nat. Nanotechnol.* **2009**, *4*, 592–597.
8. Wang, P.; Zakeeruddin, S. M.; Moser, J. E.; Nazeeruddin, M. K.; Sekiguchi, T.; Grätzel, M. A Stable Quasi-Solid-State Dye-Sensitized Solar Cell with an Amphiphilic Ruthenium Sensitizer and Polymer Gel Electrolyte. *Nat. Mater.* **2003**, *2*, 402–407.
9. Nazeeruddin, M. K.; Bessho, T.; Cevey, L.; Ito, S.; Klein, C.; De Angelis, F.; Fantacci, S.; Comte, P.; Liska, P.; Imai, H.; *et al*. A High Molar Extinction Coefficient Charge Transfer Sensitizer and its Application in Dye-Sensitized Solar Cell. *J. Photochem. Photobiol. A: Chem.* **2007**, *185*, 331–337.
10. Grätzel, M. Recent Advances in Sensitized Mesoscopic Solar Cells. *Acc. Chem. Res.* **2009**, *42*, 1788–1798.
11. Mora-Seró, I. n.; Bisquert, J. Breakthroughs in the Development of Semiconductor-Sensitized Solar Cells. *J. Phys. Chem. Lett.* **2010**, *1*, 3046–3052.
12. Sambur, J. B.; Novet, T.; Parkinson, B. A. Multiple Exciton Collection in a Sensitized Photovoltaic System. *Science* **2010**, *330*, 63–66.
13. Dang, X.; Yi, H.; Ham, M.-H.; Qi, J.; Yun, D. S.; Ladewski, R.; Strano, M. S.; Hammond, P. T.; Belcher, A. M. Virus-Templated Self-Assembled Single-Walled Carbon Nanotubes for Highly Efficient Electron Collection in Photovoltaic Devices. *Nat. Nanotechnol.* **2011**, *6*, 377–384.
14. Atwater, H. A.; Polman, A. Plasmonics for Improved Photovoltaic Devices. *Nat. Mater.* **2010**, *9*, 205–213.
15. Stuart, H. R.; Hall, D. G. Island Size Effects in Nanoparticle-Enhanced Photodetectors. *Appl. Phys. Lett.* **1998**, *73*, 3815–3817.
16. Schaadt, D. M.; Feng, B.; Yu, E. T. Enhanced Semiconductor Optical Absorption *via* Surface Plasmon Excitation in Metal Nanoparticles. *Appl. Phys. Lett.* **2005**, *86*, 063106–3.
17. Derkacs, D.; Lim, S. H.; Matheu, P.; Mar, W.; Yu, E. T. Improved Performance of Amorphous Silicon Solar Cells *via* Scattering from Surface Plasmon Polaritons in Nearby Metallic Nanoparticles. *Appl. Phys. Lett.* **2006**, *89*, 093103–3.
18. Pillai, S.; Catchpole, K. R.; Trupke, T.; Green, M. A. Surface Plasmon Enhanced Silicon Solar Cells. *J. Appl. Phys.* **2007**, *101*, 093105–8.
19. Wu, J.-L.; Chen, F.-C.; Hsiao, Y.-S.; Chien, F.-C.; Chen, P.; Kuo, C.-H.; Huang, M. H.; Hsu, C.-S. Surface Plasmonic Effects of Metallic Nanoparticles on the Performance of Polymer Bulk Heterojunction Solar Cells. *ACS Nano* **2011**, *5*, 959–967.
20. Westphalen, M.; Kreibig, U.; Rostalski, J.; Lüth, H.; Meissner, D. Metal Cluster Enhanced Organic Solar Cells. *Sol. Energy Mater. Sol. Cells* **2000**, *61*, 97–105.
21. Rand, B. P.; Peumans, P.; Forrest, S. R. Long-Range Absorption Enhancement in Organic Tandem Thin-Film Solar Cells Containing Silver Nanoclusters. *J. Appl. Phys.* **2004**, *96*, 7519–7526.
22. Morfa, A. J.; Rowlen, K. L.; Reilly, T. H.; Iii; Romero, M. J.; van de Lagemaat, J. Plasmon-Enhanced Solar Energy Conversion in Organic Bulk Heterojunction Photovoltaics. *Appl. Phys. Lett.* **2008**, *92*, 013504–3.
23. Konda, R. B.; Mundle, R.; Mustafa, H.; Bamiduro, O.; Pradhan, A. K.; Roy, U. N.; Cui, Y.; Burger, A. Surface Plasmon Excitation *via* Au Nanoparticles in n-CdSe/p-Si Heterojunction Diodes. *Appl. Phys. Lett.* **2007**, *91*, 191111–3.
24. Ihara, M.; Tanaka, K.; Sakaki, K.; Honma, I.; Yamada, K. Enhancement of the Absorption Coefficient of *cis*-$(NCS)_2$ Bis(2,2′-bipyridyl-4,4′-dicarboxylate)ruthenium(II) Dye in Dye-Sensitized Solar Cells by a Silver Island Film. *J. Phys. Chem. B* **1997**, *101*, 5153–5157.
25. Ishikawa, K.; Wen, C. J.; Yamada, K.; Okubo, T. The Photocurrent of Dye-Sensitized Solar Cells Enhanced by the Surface Plasmon Resonance. *J. Chem. Eng. Jpn.* **2004**, *37*, 645–649.
26. Hagglund, C.; Zach, M.; Kasemo, B. Enhanced Charge Carrier Generation in Dye Sensitized Solar Cells by Nanoparticle Plasmons. *Appl. Phys. Lett.* **2008**, *92*, 013113–3.
27. Standridge, S. D.; Schatz, G. C.; Hupp, J. T. Toward Plasmonic Solar Cells: Protection of Silver Nanoparticles *via* Atomic Layer Deposition of TiO_2. *Langmuir* **2009**, *25*, 2596–2600.
28. Standridge, S. D.; Schatz, G. C.; Hupp, J. T. Distance Dependence of Plasmon-Enhanced Photocurrent in Dye-Sensitized Solar Cells. *J. Am. Chem. Soc.* **2009**, *131*, 8407–8409.
29. Zhao, G.; Kozuka, H.; Yoko, T. Effects of the Incorporation of Silver and Gold Nanoparticles on the Photoanodic Properties of Rose Bengal Sensitized TiO_2 Film Electrodes Prepared by Sol-Gel Method. *Sol. Energy Mater. Sol. Cells* **1997**, *46*, 219–231.
30. Wen, C.; Ishikawa, K.; Kishima, M.; Yamada, K. Effects of Silver Particles on the Photovoltaic Properties of Dye-Sensitized TiO_2 Thin Films. *Sol. Energy Mater. Sol. Cells* **2000**, *61*, 339–351.
31. Ding, I. K.; Zhu, J.; Cai, W.; Moon, S.-J.; Cai, N.; Wang, P.; Zakeeruddin, S. M.; Grätzel, M.; Brongersma, M. L.; Cui, Y.; *et al*. Plasmonic Back Reflectors: Plasmonic Dye-Sensitized Solar Cells. *Adv. Energy Mater.* **2011**, *1*, 51–51.
32. Brown, M. D.; Suteewong, T.; Kumar, R. S. S.; D'Innocenzo, V.; Petrozza, A.; Lee, M. M.; Wiesner, U.; Snaith, H. J. Plasmonic Dye-Sensitized Solar Cells Using Core−Shell Metal−Insulator Nanoparticles. *Nano Lett.* **2010**, *11*, 438–445.

33. Willets, K. A.; Van Duyne, R. P. Localized Surface Plasmon Resonance Spectroscopy and Sensing. *Annu. Rev. Phys. Chem.* **2007**, *58*, 267–297.
34. Kelly, K. L.; Coronado, E.; Zhao, L. L.; Schatz, G. C. The Optical Properties of Metal Nanoparticles: The Influence of Size, Shape, and Dielectric Environment. *J. Phys. Chem. B* **2002**, *107*, 668–677.